Journal of
Ceramic Science
and Technology

J. Ceram. Sci. Tech., **06** [02] 119-124 (2015)
DOI: 10.4416/JCST2014-00033
available online at: http://www.ceramic-science.com

Functionally Graded Ceramic Structures by Direct Thermal Inkjet Printing

P. Gingter*, A.M. Wätjen, M. Kramer, R. Telle

Department of Ceramics and Refractory Materials,
RWTH Aachen University, Mauerstraße 5, 52064 Aachen, Germany

received August 15, 2014; received in revised form September 12, 2014; accepted October 1, 2014

Abstract

Aqueous inks based on fine alumina and zirconia powder (3Y-TZP) with a solids content of 21 vol% were developed and adapted to a direct inkjet printing (DIP) system by optimizing the solids content, surface tension and viscosity of the inks. Using different thermal printheads for alumina and 3Y-TZP ink, dispersion ceramics and functionally graded materials (FGM) were generated via precise dropwise combination of materials on a substrate. Green and sintered specimens feature high density and accuracy with regard to drop positioning, which underlines the high potential of DIP for the fabrication of functionally graded ceramic structures.

Keywords: Direct inkjet printing, suspensions, functionally graded materials, ZrO_2, Al_2O_3

I. Introduction

Predefined combinations of ceramic materials are commonly termed dispersion ceramics if one phase is homogeneously dispersed in another one. Such material combinations can be assigned to the group of functionally graded materials (FGM) if the composition is continuously varied across the volume [1,2]. FGM can be found in natural materials like bones, nacre and wood, where material and structural efficiency has been evolutionarily optimized based on local adaption of the microstructure to external requirements [3]. A gradual change of material composition within one component is very promising for applications in electronics, aeronautics or medicine, which require position-dependent properties [4–6]. In this context, the mixture of alumina and 3Y-TZP is a promising material system, as these oxide ceramics are biocompatible and show excellent hardness and strength, respectively [7]. By combining these materials, properties that feature specific characteristics of both alumina and 3Y-TZP can be achieved [8]. Parts containing a graded composition possess locally different properties. Hence the accurate spatial control of the material composition is crucial. Conventional processing techniques such as slip casting [9], electrophoretic deposition [10], or low-pressure joining [11] are limited in this regard, as graded structures can only be realized in a discrete manner or part geometries are limited to simple shapes.

Additive manufacturing technologies such as stereolithography [12], selective laser sintering [13], three-dimensional printing [14] and fused deposition modelling are used to build complex three-dimensional ceramic parts layer by layer directly from a computer aided design (CAD) model without the need for molds or part-specific tools. In terms of functionally graded materials, these techniques benefit from their flexibility in manufacturing as well as the possibilities in specifying material compositions. Direct inkjet printing (DIP) has an exceptional position within additive manufacturing, as material is added dropwise in a direct manner [15]. Inks containing ceramic particles and functional additives like surfactants, binders and humectants are ejected through fine nozzles, whose diameters are typically in a range of 20–30 µm [16]. By placing the building material in pico-liter-sized droplets, geometry and composition of parts can be specified accurately [17,18]. Different rules of thumb have been proposed, which suggest the ratio of nozzle orifice to particle diameter should be larger than 50, or 100, respectively [19,20]. The solid content has to be above 20 vol% to enable defect-free, efficient layer-wise production of parts [21].

To ensure reliable drop ejection without the formation of satellite droplets, density, viscosity and surface tension of the suspensions have to be adjusted precisely to the particular printheads used. The inverse of the dimensionless Ohnesorge number (Oh^{-1}), which relates inertial and surface forces to viscous forces, is often used to describe the behavior of fluids in printing processes:

$$Oh^{-1} = \frac{\sqrt{\sigma \cdot \rho \cdot a}}{\eta} \qquad (1)$$

where σ, ϱ and η represent the density, dynamic surface tension and dynamic viscosity of the ink, respectively and a is the characteristic length (the nozzle radius of the printhead). Concerning piezoelectric printheads, it has been demonstrated that Oh^{-1} should be in the range of $1 < Oh^{-1} < 10$, in which reliable ejection of flawless, single drops is ensured [15,18,22,23]. For thermal printheads however, no clear quantitative correlation between Oh^{-1} and drop integrity exists [24,25]. Ceramic inks with a viscosity up to

* Corresponding author: gingter@ghi.rwth-aachen.de

15 mPa s have been printed with thermal printheads, while the dynamic surface tension was adjusted in a range of 35 – 52 mN m^{-1} to create drops without the occurrence of satellite droplets [24,25].

Inks of oxide as well as non-oxide ceramics have been developed and three-dimensional structures like micro pillar arrays, thin walls or gearwheels have been printed [21,26–27]. Components feature high green and sintered density and thus demonstrate excellent mechanical properties. Consequently, DIP is qualified for the construction of individual, complex-shaped functional and structural ceramics, such as channel structures, microelectronic components, dental crowns or bridges [16–19,22–23,25–31]. Printed structures may even feature cavities or undercuts [32]. Parts which are functionally graded along one axis with continuously varying material distribution have been produced by using an ink mixing protocol before drop ejection [33,34]. The fabrication of FGM by use of diverse printheads for different materials has been suggested for flat exemplary structures [35].

The objective of this study is to realize three-dimensional dispersion ceramics and FGM of alumina and 3Y-TZP by using DIP. Structures are built up via precise dropwise combination of materials on the substrate by implementing different printheads for alumina and 3Y-TZP as shown schematically in Fig. 1. Ceramic inks are characterized with regard to particle size distribution, solids content, viscosity and surface tension as well as printing performance. Parts are analyzed in respect of density, microstructure and composition.

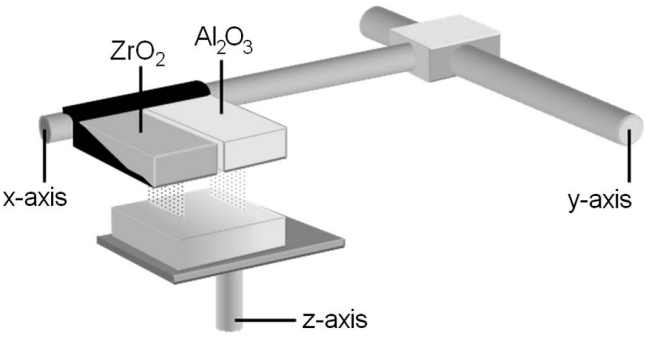

Fig. 1: Scheme of parallel direct inkjet printing with two printheads.

II. Experimental Procedure

(1) Preparation and characterization of ceramic inks

Aqueous inks of Al_2O_3 (BA15PSH, Baikowski Group, Annecy, France) and 3Y-TZP (TZ-3YS-E, Tosoh Corporation, Yamaguchi, Japan) with solid contents of 21 vol%, respectively, were prepared. 3Y-TZP powder with a mean particle size of 600 nm was dispersed and ground for eight hours at 2500 rpm with a laboratory agitator bead mill (MicroCer, NETZSCH-Feinmahltechnik, Selb, Germany) using zirconia grinding balls (diameter 50 µm). Particles were stabilized electrosterically by means of the addition of 0.5 wt% (related to solids) carboxylic acid (Dolapix CE64, Zschimmer & Schwarz, Lahnstein, Germany). Al_2O_3 was provided as aqueous dispersion with a mean particle size of 146 nm. The suspension was already stabilized electrostatically at pH 4.6 by the manufacturer. With the addition of ethanol, ethylene glycol (Merck KGaA, Darmstadt, Germany), binder (PEG 400, Merck KGaA, Darmstadt, Germany) and an anti-foaming agent (Contraspum, Zschimmer & Schwarz, Lahnstein, Germany) the inks were adapted to the printing system. Printing performance was analyzed using single-drop experiments. Here, single droplets were printed on polished green alumina and 3Y-TZP substrates, respectively and drop integrity was analyzed optically after the printing process without any further treatment. Subsequently, the inks were further optimized to avoid formation of satellite drops. Detailed optimization procedure of ceramic inks for direct inkjet printing has been reported elsewhere [21]. The final composition of both optimized inks is given in Table 1.

The particle size distribution was analyzed by means of the laser diffraction technique (Mastersizer 2000, Malvern Instruments, Worcestershire, UK). The dynamic viscosity of the inks at 20 °C was determined using a rheometer with concentric cylinder measuring system (RheolabQC with double gap cylinder DG 42, Anton Paar, Graz, Austria) at shear rates of 1000 1/s. A bubble pressure tensiometer (SITA pro line t15, SITA Messtechnik, Dresden, Germany) was used to measure the dynamic surface tension at 20 °C. The pH values of the inks were determined using a pH-electrode (InLab 417, Mettler Toledo, Giessen, Germany)

Table 1: Composition of Al_2O3- and 3Y-TZP-inks.

Material	Al_2O_3-ink		3Y-TZP-ink	
	Content (wt%)	Content (vol%)	Content (wt%)	Content (vol%)
Ceramic powder	51.9	21.0	62.5	21.0
Distilled water	28.0	44.3	21.6	43.9
Dispersant	-	-	0.3	0.5
Ethanol	10.5	21.0	8.1	20.9
Ethylene glycol	7.0	10.0	5.5	10.0
Binder	2.5	3.5	1.9	3.5
Anti-foaming agent	0.1	0.2	0.1	0.2

(2) Printer modification and printing procedure

Graded structures were realized by direct printing of combinations of alumina and 3Y-TZP inks. By means of parallel printing with two separate thermal drop-on-demand printheads, the materials were combined on the substrate. The printing unit is based on a conventional 3D powder bed printer with three movable axes (Z510, Z-Corporation, Burlington, USA), which was modified for the requirements of DIP, as presented in Fig. 2. The printer is equipped with four separate printheads (transparent, cyan, magenta, yellow) each with 302 nozzles of 24 µm in diameter arranged in two parallel rows, providing a resolution of 600 x 540 dpi (HP 11 printheads, Hewlett-Packard, Palo Alto, USA). By default, in 3D powder bed printing, aqueous binders (ZB 60 binder, Z-Corporation, Burlington, USA) selectively join the particles of the powder bed. These inks do not contain any particles and thus significantly differ from the developed ceramic inks in respect of physical and chemical characteristics. For DIP of particulate suspensions, an additional printhead cleaning system and a more accurate z-axis, which allows movements of a few micrometers, were added to the printer. This precision is needed for DIP, where the layer thickness is below ten micrometers [16]. The deposition of each layer was followed by evaporation of the volatile ink contents and the substrate was lowered before printing the next layer. A supplementary fan heater was attached to ensure satisfying drying rates at substrate temperatures of 80 °C.

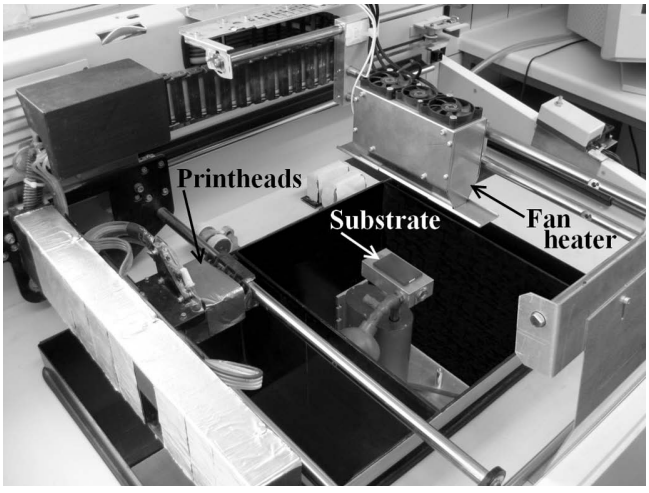

Fig. 2: Modified 3D printer including z-axis with higher accuracy and adapted drying and cleaning unit.

3D modeling software (Rhinoceros 4, Robert McNeel & Associates, Seattle, USA) was used for the generation of three-dimensional models using the printer-compatible file format vrml, which allows the creation of models with colored surfaces. As the interior of these files do not contain color information, three-dimensional parts are realized by repeatedly printing the upper surface of the part on top of each other. In our case two printheads were used, each filled with a different ceramic ink. The yellow printhead was responsible for alumina ink, while the cyan printhead was applied to print 3Y-TZP ink. Using this color codification, dispersion ceramics and functionally graded structures have been realized. Certain material (color) combinations are obtained by placing single drops of the base materials (colors) next to another on the substrate, which is done independently by the printing system. Here, the printing system uses an algorithm for the translation of optical color impression to the corresponding volume of ink to be printed, which is not accessible to the user.

FGM parts were designed as rectangle with a length and width of 30 mm and 8.5 mm, respectively. The parts feature a color gradient from 100 % yellow to 100 % cyan. The dispersion ceramics with fixed alumina-3Y-TZP ratio were designed as cylinders with a diameter of 10 mm. The intended ratio of 82.3 vol% alumina to 17.7 vol% 3Y-TZP was realized by printing cylinders, whose base area was colored with following color values (RGB): 200; 255; 0.

(3) Sintering

The printed structures were dried at 80 °C for 24 h. The parts were placed into a powder bed and organic additives were pyrolyzed at 850 °C for 1 h at a heating rate of 2 K/min. Subsequently, they were sintered at 1550 °C for 2 h at the same heating rate. Debinding and sintering were performed in one process cycle in a resistance-heated high-temperature chamber furnace (HT 64/17, Nabertherm, Lilienthal, Germany).

(4) Characterization of green and sintered bodies

The green and sintered structures were optically analyzed by means of light microscopy (Zeiss Stemi 2000-CS, Carl Zeiss AG, Oberkochen, Germany) and SEM (Leo 440i, Leo Elektronenmikroskopie GmbH, Oberkochen, Germany). Back-scattered electron (BSE) images were used to characterize the printed structures with regard to droplet placement of individual materials. The chemical composition of the materials was analyzed with energy-dispersive x-ray spectroscopy (EDS). Sintered parts were polished rectangular to the direction of layer-wise build-up to study the microstructure. The density of the sintered specimens was determined using the principle of Archimedes.

III. Results

(1) Characteristics of ceramic inks

Grinding of 3Y-TZP resulted in a particle size of ~ 200 nm (d_{90}) after 8 h grinding time. Further grinding did not significantly reduce the particle size. Alumina was already dispersed in aqueous media and stabilized electrostatically, with a particle size of 193 nm (d_{90}). Laser diffraction analysis shows a slightly broader particle size distribution of the final 3Y-TZP-ink, compared to the final alumina ink as Fig. 3 illustrates. Both inks were long-time stable and clogging of nozzles or feed-channels of the printheads due to coarse particles or agglomerates was not observed. The single-drop experiments revealed the importance of adapting dynamic surface tension and viscosity in order to avoid satellite droplets and to guarantee a sharp print image. Fig. 4 shows the results of single-drop experiments for alumina ink before (Fig. 4a) and

after (Fig. 4b) the optimization procedure. The dynamic viscosity of optimized alumina and 3Y-TZP ink was measured as 4.5 and 4.8 mPa s, respectively, at a shear rate of 1000 1/s. Neither ink showed any thixotropic behavior. The viscosities of ceramic inks were similar, however, slightly higher than the viscosity of the standard binder for 3D printing with a value of 1.9 mPa s at the same shear rate. The dynamic surface tension at bubble lifetimes of 100 ms was determined to be 47.9 mN m^{-1} for the alumina ink and 50.3 mN m^{-1} for the 3Y-TZP ink, which was considerably above the standard binder with a surface tension of 33.5 mN m^{-1}.

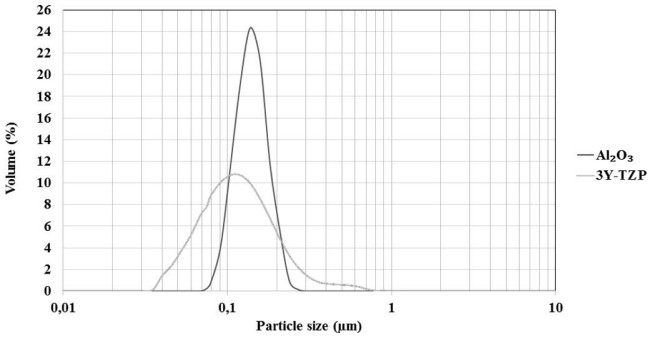

Fig. 3: Particle size distribution of final 3Y-TZP- and Al_2O_3-inks.

(2) Printing performance and characteristics of printed structures

The modified 3D powder bed printer was suitable for DIP of ceramic suspensions. Compared to previous studies, this printing unit features an additional movable axis in y-direction, which potentially enables the production of large-scale parts [16, 21, 27–31]. The z-axis permits movements of a few micrometers, which provides the precision needed for DIP. The attached cleaning device reliably removed adhering ink residues from the printhead nozzle plate, which is important to prevent exterior caking on the nozzles. A substrate temperature of 80 °C was generated by the external fan heater to guarantee a fast and uniform drying process. No drying cracks or warping of layers could be identified on the printed structures.

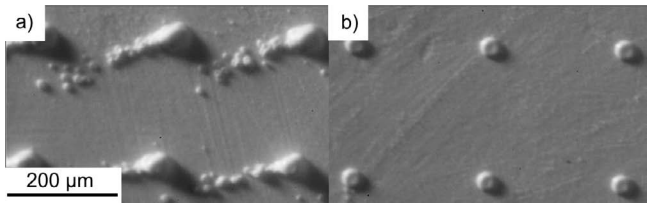

Fig. 4: Single-drop evaluation of alumina ink: a) before ink optimization; b) after ink optimization.

Graded structures were realized by building up parts based on a rectangular model with a colored surface of yellow and cyan (Fig. 5a). Three-dimensional parts were built up by multiple-printing of the top surface of the graded color model. The application of the color codification described above (yellow = alumina, cyan = 3Y-TZP), resulted in a continuously varying material distribution. Fig. 5b shows a BSE image of the top view of the printed green body with the alumina-rich part on the right side and the 3Y-TZP-rich part on the left side. This graded green structure was analyzed using EDS, which showed that the profile widely corresponds to the specified pattern. However, a slightly disproportionately high amount of alumina was printed throughout the entire area, while the content of 3Y-TZP was marginally lower than expected (Fig. 6). Nevertheless, the gradient shows a stepless changeover from 100 per cent alumina to 100 per cent 3Y-TZP.

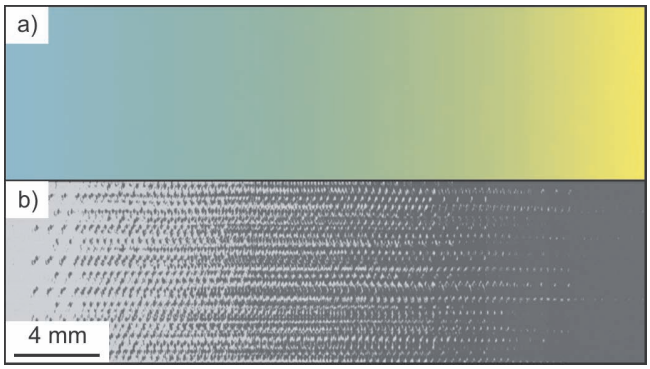

Fig. 5: Rectangular functionally graded structure: a) graded color model b) BSE image of resulting material gradient (green body) from 3Y-TZP (left) to Al_2O_3 (right).

Eight cylindrical parts with fixed alumina-3Y-TZP ratios were printed, showing similar results as described above for the rectangular gradient parts with regard to disproportional ink combination. The parts with a diameter of 10 mm are shown in Fig. 7. SEM analyses of the sintered cylindrical parts reveal a dense microstructure and a regular arrangement of 3Y-TZP droplets inside the alumina matrix, as shown in the cross-sectional view of Fig. 8. The optical analysis of the 3Y-TZP droplets revealed a single-layer thickness of ~ 2 µm and a mean droplet diameter of ~ 70 µm after sintering, respectively. The microstructure does not show single, disconnected layers, or other defects resulting from additive manufacturing, although the specimens consist of 800 successively deposited single layers. The density of the parts was measured to be between 95.7 and 97.5 % of the theoretical density, which was calculated based on EDS area analyses as 4.29 g/cm^3.

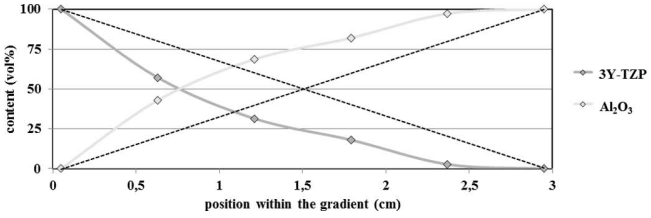

Fig. 6: Gradient of Al_2O_3 (yellow) -3Y-TZP (cyan) as measured by means of EDS, with intended profiles (dashed lines).

Fig. 7: Green Al_2O_3-3Y-TZP cylinders consisting of 800 layers.

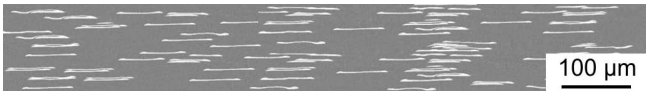

Fig. 8: SEM micrograph of sintered Al_2O_3-3Y-TZP cylinder (cross-section).

IV. Discussion

The particle size distributions of alumina and 3Y-TZP, which were measured by laser diffraction, show that the rules of thumb proposed by Lejeune and Magdassi are both satisfied [19,20]. Both types of powder show a ratio of nozzle orifice to particle size of ~120. As a result no further grinding of the as-received alumina suspension was necessary and grinding of 3Y-TZP suspension was stopped after 8 h.

Small variations of ethanol, ethylene glycol, polyethylene glycol and humectant have significant influence on printing performance, underlining the sensibility of ceramic inks in DIP [16,21]. After optimization of the additive system, both 3Y-TZP and alumina inks were flawlessly jettable using the modified 3D printer, as shown exemplarily for alumina ink in Fig. 4. Dilution of ceramic inks significantly reduces viscosity, which is beneficial for DIP with regard to the refilling mechanism inside the printhead [20]. On the contrary, low viscosities may induce sedimentation of particles due to agglomeration. Although viscosities were below 5 mPa s for both ceramic inks no agglomeration of particles and no blockage of feed channels or nozzles were observed, revealing a successful dispersion of alumina and 3Y-TZP inks by electrostatical and electrosterical mechanisms, respectively. The solids content of 21 vol% was slightly lower than in previous studies but it was still adequate for the layer-wise build-up of parts. The layer thickness of ~2 µm (analyzed after sintering) corresponds to a faster drying, which has contributed to the generation of three-dimensional components, without the occurrence of drying defects. Flaws such as cracks or bulged layers have been observed for inks with low solid contents or for decelerated drying [21,36].

The dynamic surface tension of both optimized ceramic inks considerably exceeds the values measured for the standard binder at bubble lifetimes of 100 ms. Nonetheless, single drops which were printed with these inks show full drop integrity, without the formation of satellite droplets. The combination of physical ink properties such as density, viscosity and surface tension has to be taken into account with regard to the optimization of drop ejection [16]. Nevertheless, until today it was not possible to develop clear quantitative relations between the drop integrity and dimensionless physical numbers such as the Reynolds, Weber, or Ohnesorge number, to describe the formation of single drops for thermal inkjet printing [16,21]. Here it was shown that an enhanced surface tension may compensate for the increase of viscosity in comparison to the standard ink, which is in accordance to the findings of Özkol [24].

The graded rectangular structures printed with the modified powder bed printer outline the potential of DIP to create three-dimensional FGM with compositional gradients. By combining alumina and 3Y-TZP after drop ejection on the substrate it was possible to achieve smooth material transitions. As compared to previous studies, where different materials were combined before drop ejection by using an ink mixing protocol, the step width of compositional changes is slightly higher in the present study [33,34]. This may be explained by the incomplete mixture of single droplets on the substrate. Immediately after drop ejection the drops begin to dry, which is even accelerated at the moment of impact on the printed layers. The smoothness of material transition therefore is limited by the size of the single drops. Nevertheless, the possibilities regarding spatial control of material composition by using this dropwise positioning may not be achieved with other methods in a similar way. With a further reduction of the droplets' size and better control of their individual position, enhanced material mixture and thus higher resolutions may be achieved in the future with DIP.

The color codification proposed here proved to be a proper method to define material composition. However, a completely precise transformation of color to material could not be achieved using the modified powder bed printer. The observation that the amount of alumina ink printed exceeded the intended level, while an insufficient amount of 3Y-TZP ink was printed may be explained by the different intensity of the basic colors yellow and cyan. As yellow is a "weak color", the algorithms of the printing system may be programmed such that the printed volume of yellow ink is higher than for cyan ink. As a result the inherent different color intensity is offset and a similarly intense color impression is obtained. To fully reveal the potential of the proposed DIP method for the production of FGM, algorithms that guarantee a drop ejection that is entirely proportional to the specified color combination should be implemented.

In addition to the slight deviation from the specified material composition the layer thickness appeared to be considerably lower than in previous studies of DIP, where ~5 µm were achieved [16,21,27–31]. Here, printing in color mode generated layer thicknesses of ~2 µm, which resulted in prolonged periods for the completion of three-dimensional parts. Nevertheless, SEM analyses revealed a homogeneous microstructure, which indicates that the printing and drying conditions were suitable for the single layers to completely bond together. Besides high edge definition, components feature nearly full density, which demonstrates that DIP is a versatile method to produce geometrically complex, three-dimensional components for applications which place high requirements on mechanical properties and spatial material composition.

V. Conclusions

A printing unit based on a commercial 3D powder bed printer was adapted for DIP of highly loaded aqueous suspensions by incorporating both cleaning and drying devices as well as a high-precision z-axis. Dispersion ceramics and functionally graded structures in the alumina-3Y-TZP system were realized by parallel direct inkjet printing with separate printheads. A color codification system was applied to define the material composition by using the elementary colors yellow and cyan for alumina and 3Y-TZP, respectively. By way of placing dots of the particular materials in juxtaposition with each other in defined, varying positions, stepless graded structures were realized. In the same way, precise, dense, three-dimensional cylindrical parts were printed, consisting of 800 single layers. After sintering, up to 97.5 % of the theoretical density was achieved. The microstructure was homogeneous

and no lamination or other process-related defects were detected. No traces of layer-wise, additive manufacturing could be found. Improvements concerning the software and control of the printing unit will permit the creation of graded structures with varying material composition in every spatial direction by means of DIP.

References

1 Erasenthiran, P., Beal, V.E.: Functionally graded materials. in: rapid manufacturing: an industrial revolution for the digital age. Wiley-VCH, Weinheim, Germany, 2006.

2 Miyamoto, Y., Kaysser, W.A., Rabin, B.H., Kawasaki, A., Ford, R.G.: Functionally graded materials: design, processing and applications. Kluwer Academic Publishers, Boston, MA, 1999.

3 Oxman, N.: Variable property rapid prototyping, *Virtual. Phys. Prototyp.,* **6**, 3 – 31, (2011).

4 Markovića, S., Jovalekićb, Č., Veselinovića, L., Mentusc, S., Uskoković, D.: Electrical properties of barium titanate stannate functionally graded materials, *J. Eur. Ceram. Soc.*, **30**, [6], 1427 – 36, (2010).

5 Ruys, A.J., Popova, E.B., Suna, D., Russella, J.J., Murray, C.C.J.: Functionally graded electrical/thermal ceramic systems, *J. Eur. Ceram. Soc.,* **21**, [10 – 11], 2025 – 9, (2001).

6 Ortmann, C., Oberbach, T., Richter, H., Puhlfürss, P.: Preparation and characterization of ZTA bioceramics with and without gradient in composition, *J. Eur. Ceram. Soc.,* **32**, [4], 777 – 85, (2012).

7 De Aza, A.H., Chevalier, J., Fantozzi, G., Schehl, M., Torrecillas, R.: Crack growth resistance of alumina, zirconia and zirconia toughened alumina ceramics for joint prostheses, *Biomaterials,* **23**, [3], 937 – 45, (2002).

8 Sun, L., Sneller, A., Kwon, P.: Fabrication of alumina/zirconia functionally graded material: from optimization of processing parameters to phenomenological constitutive models, *Mat. Sci. Eng. A-Struc.,* **488**, [1 – 2], 31 – 8, (2008).

9 He, X., Du, H., Wang, W., Jing, W., Liu, C.: Fabrication of ZrO_2-SUS functionally graded materials by slip casting, *Key. Eng. Mater.,* **368 – 372**, 1823 – 4, (2008).

10 Askari, E., Mehrali, M., Metselaar, I.H., Kadri, N.A., Rahman, M.M.: Fabrication and mechanical properties of Al_2O_3/SiC/ZrO_2 functionally graded material by electrophoretic deposition, *J. Mech. Behav. Biomed. Mater.*, **12**, 144 – 50, (2012).

11 Gurauskis, J., Sánchez-Herencia, A.J., Baudín, C.: Laminated ceramic structures within alumina/YTZP system obtained by low pressure joining, *Key. Eng. Mater.*, **333**, 219 – 22, (2007).

12 Cicha, K., Li, Z., Stadlmann, K., Ovsianikov, A., Markut-Kohl, R., Liska, R., Stampfl, J.: Evaluation of 3D structures fabricated with two-photon-photopolymerization by using FTIR spectroscopy, *J. Appl. Phys.*, **110**, 1 – 5, (2011).

13 Bourell, D.L., Marcus, H.L., Barlow, J.W., Beamann, J.J.: Selective laser sintering of metals and ceramics, *Int. J. Powder. Metall.*, **28**, 369 – 81, (1992).

14 Sachs, E.M., Cima, M.J., Cornie, J.: Three-dimensional printing: rapid tooling and prototypes directly from a CAD model, *CIRP. Ann. Manuf. Technol.*, **39**, 201 – 4, (1990).

15 Lewis, J.A., Smay, J.E., Stuecker, J., Cesarano III, J.: Direct ink writing of three-dimensional ceramic structures, *J. Am. Ceram. Soc.*, **89**, [12], 3599 – 609, (2006).

16 Özkol, E., Ebert, J., Uibel, K., Wätjen, A.M., Telle, R.: Development of high solid content aqueous 3Y-TZP suspensions for direct inkjet printing using a thermal inkjet printer, *J. Eur. Ceram. Soc.*, **29**, [3], 403 – 9, (2009).

17 Zhao, X., Evans, J.R.G., Edirisinghe, M.J., Song, J.H.: Ink-jet printing of ceramic pillar arrays, *J. Mater. Sci.*, **37**, 1987 – 92, (2002).

18 Derby, B., Reis, N.: Inkjet printing of highly loaded particulate suspensions, *MRS Bull.*, **28**, 815 – 8, (2003).

19 Lejeune, M., Chartier, T., Dossou-Yovo, C., Noguera, R.: Ink-jet printing of ceramic micro pillar arrays, *J. Eur. Ceram. Soc.*, **29**, 905 – 11, (2009).

20 Magdassi, S.: The chemistry of inkjet inks. World Scientific Publishing Co., Singapore, 2010.

21 Özkol, E., Ebert, J., Telle, R.: An experimental analysis of the influence of the ink properties on the drop formation for direct thermal inkjet printing of high solid content aqueous 3Y-TZP suspensions, *J. Eur. Ceram. Soc.*, **30**, [7], 1669 – 78, (2010).

22 Seerden, K.A.M., Reis, N., Evans, J.R.G., Grant, P.S., Halloran, J.W., Derby, B.: Ink-jet printing of wax-based alumina suspensions, *J. Am. Ceram. Soc.*, **84,** [11], 2514 – 20, (2001).

23 Noguera, R., Lejeune, M., Chartier, T.: 3D fine scale ceramic components formed by ink-jet prototyping process, *J. Eur. Ceram. Soc.*, **25**, [12], 2055 – 9, (2005).

24 Özkol, E.: Rheological characterization of aqueous 3Y-TZP inks optimized for direct thermal ink-jet printing of ceramic components, *J. Am. Ceram. Soc.*, **96**, [4], 1124 – 30, (2013).

25 Cappi, B., Ebert, J., Telle, R.: Rheological properties of aqueous Si_3N_4 and $MoSi_2$ suspensions tailor-made for direct inkjet printing, *J. Am. Ceram. Soc.*, **94**, 111 – 6, (2011).

26 Zhao, X., Evans, J.R.G., Edirisinghe, M.J., Song, J.H.: Direct ink-jet printing of vertical walls, *J. Am. Ceram. Soc.*, **85**, [8], 2113 – 5, (2002).

27 Cappi, B., Özkol, E., Ebert, J., Telle, R.: Direct inkjet printing of Si_3N_4: characterization of ink, green bodies and microstructure, *J. Eur. Ceram. Soc.,* **28**, [13], 2625 – 8, (2008).

28 Ebert, J., Özkol, E., Telle, R., Fischer, H., Uibel, K.: Direct inkjet printing: A versatile method of complex shape manufacturing. In: Proceedings of the 10th European Ceramic Society Conference. Göller Verlag GmbH, Baden-Baden, Germany, 2008.

29 Özkol, E., Wätjen, A.M., Bermejo, R., Deluca, M., Ebert, J., Danzer, R., Telle, R.: Mechanical characterisation of miniaturised direct inkjet printed 3Y-TZP specimens for microelectronic applications, *J. Eur. Ceram. Soc.*, **30**, [15], 3145 – 52, (2010).

30 Ebert, J., Özkol, E., Zeichner, A., Uibel, K., Weiss, Ö., Koops, U., Telle, R., Fischer, H.: Direct inkjet printing of dental prostheses made of zirconia, *J. Dent. Res.*, **88**, [7], 673 – 6, (2009).

31 Özkol, E., Zhang, W., Ebert, J., Telle, R.: Potentials of the "direct inkjet printing" method for manufacturing 3Y-TZP based dental restorations, *J. Eur. Ceram. Soc.*, **32**, [10], 2193 – 201, (2012).

32 Mott, M., Song, J.H., Evans, J.R.G.: Microengineering of ceramics by direct ink-jet printing, *J. Am. Ceram. Soc.*, **82**, [7], 1653 – 8, (1999).

33 Mott, M., Evans, J.R.G.: Zirconia/alumina functionally graded material made by ceramic ink jet printing, *Mater. Sci. Eng.*, **271**, 344 – 52, (1999).

34 Mohebi, M.M., Evans, J.R.G.: A Drop-on-demand ink-jet printer for combinatorial libraries and functionally graded ceramics, *J. Comb. Chem.*, **4**, [4], 267 – 74, (2002).

35 Wang, J., Shaw, L.L.: Fabrication of functionally graded materials via inkjet color printing, *J. Am. Ceram. Soc.*, **89**, [10], 3285 – 9, (2006).

36 Song, J.H., Nur, H.M.: Defects and prevention in ceramic components fabricated by inkjet printing, *J. Mater. Proc. Technol.*, **155**, [6], 1286 – 92, (2004).